

Sub-10 Femtosecond Intervalley Exciton Coupling in Monolayer MoS₂ Revealed by Helicity-Resolved Two-Dimensional Electronic Spectroscopy

Lawson T. Lloyd,^{1,2,3} Ryan E. Wood,^{1,2,3} Fauzia Mujid,^{1,2} Siddhartha Sohoni,^{1,2,3} Karen L. Ji,^{1,2,3} Po-Chieh Ting,^{1,2,3} Jacob S. Higgins,^{1,2,3} Jiwoong Park,^{1,2,4} and Gregory S. Engel^{1,2,3,}*

¹Department of Chemistry, The University of Chicago, Chicago, Illinois, 60637, USA

²James Franck Institute, The University of Chicago, Chicago, Illinois, 60637, USA

³Institute for Biophysical Dynamics, The University of Chicago, Chicago, Illinois, 60637, USA

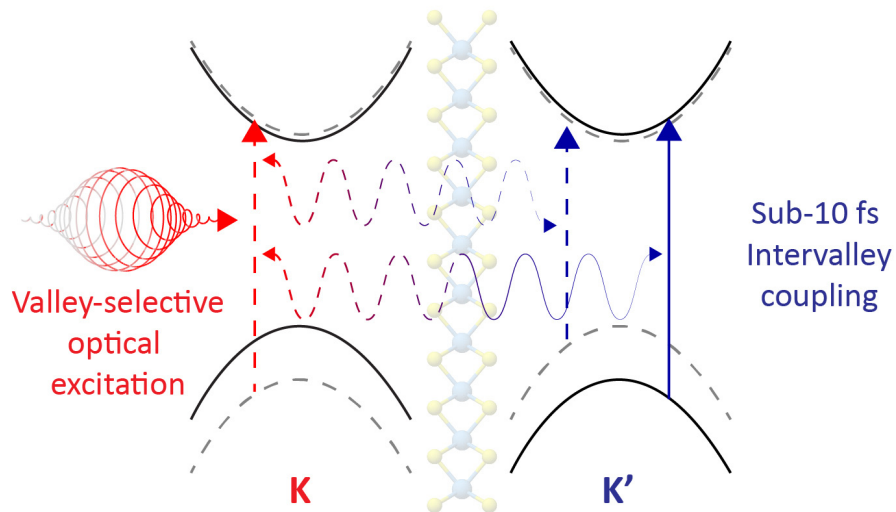
⁴Pritzker School of Molecular Engineering, The University of Chicago, Chicago, Illinois, 60637, USA

*gsengel@uchicago.edu

ABSTRACT: The valley pseudospin at the K/K' high symmetry points in monolayer transition-metal dichalcogenides (TMDs) has potential as an optically addressable degree of freedom in next-generation optoelectronics. However, intervalley scattering and relaxation of charge carriers leads to valley depolarization and limits practical applications. In addition, enhanced Coulomb interactions lead to pronounced excitonic effects that dominate the optical response and initial valley depolarization dynamics, but complicate the interpretation of ultrafast spectroscopic experiments at short time delays. Employing broadband helicity-resolved two-dimensional electronic spectroscopy

(2DES), we observe ultrafast (~ 10 fs) intervalley coupling between all A and B valley exciton states that results in a complete breakdown of the valley index in large-area monolayer MoS₂ films. These couplings and subsequent dynamics exhibit minimal excitation fluence or temperature dependence and are robust to changes in sample grain size and inherent strain. Our observations strongly suggest that this direct intervalley coupling on the timescale of optical excitation is an inherent property of large-area MoS₂ distinct from dynamic carrier or exciton scattering, phonon-driven processes, and multiexciton effects. This ultrafast intervalley coupling poses a fundamental challenge for exciton-based valleytronics in monolayer TMDs and must be overcome to fully realize large-area valleytronic devices.

KEYWORDS: *valleytronics, transition-metal dichalcogenides, 2D materials, two-dimensional spectroscopy, ultrafast spectroscopy, exciton dynamics*



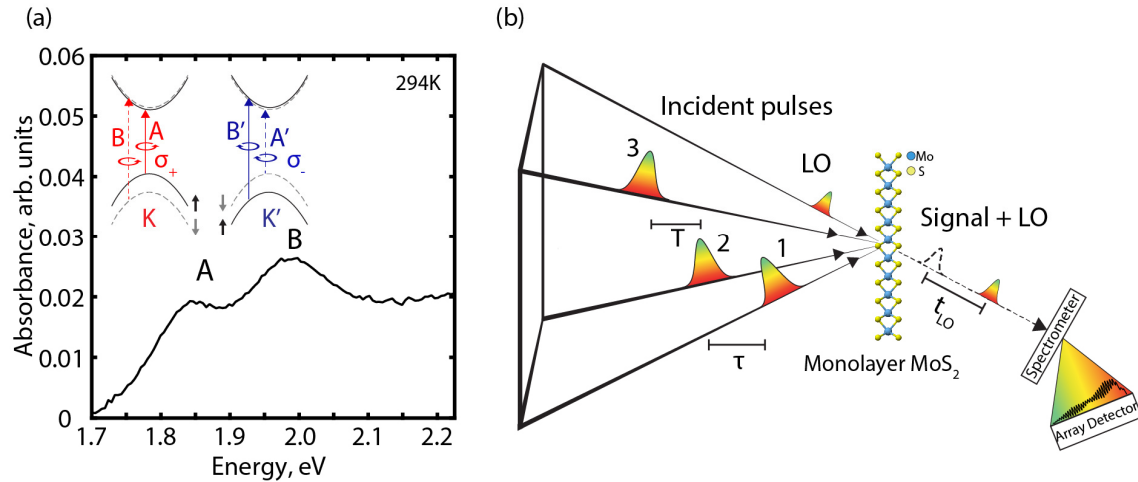


Figure 1. Monolayer MoS₂ linear absorption and 2DES experimental geometry. (a) Linear absorption spectrum of MOCVD-grown monolayer MoS₂ resolves two prominent exciton peaks (A and B) with opposite circularly polarized optical transitions σ_+/σ_- at the K/K' points (inset). (b) Three broadband femtosecond pulses (1-3) incident on a sample in the 'BOXCARS' geometry generate a third-order nonlinear signal in the phase-matched direction collinear to a fourth attenuated pulse, the local oscillator (LO), used in heterodyne detection. The LO precedes the excitation beams and generated signal by $t_{LO} \sim 1300$ fs. The heterodyned signal is spectrally dispersed onto an array detector to resolve the detection energy (note the interferogram). The excitation energy is resolved by Fourier transformation of the first scanned time delay, τ . Population dynamics are probed by scanning the second time delay, T .

TMD monolayers (MX₂ : M = Mo, W ; X = S, Se) and stacked heterostructures have gained considerable interest as atomically thin and flexible components in next-generation photonic and optoelectronic applications,¹⁻³ owing in large part to the distinct electronic and optical properties that emerge in the monolayer limit. These properties include a transition to a direct band gap,^{4,5} strong excitonic effects,⁶⁻⁸ and nonequivalent band extrema, or valleys, in reciprocal space.^{9,10} Quantum confinement and reduced dielectric screening lead to Coulombically bound electron-hole pairs, or excitons, with binding energies on the order of ~ 500 meV as well as robust multi-exciton complexes even at room-temperature.¹¹⁻¹³ Broken inversion symmetry and large spin-orbit coupling give rise to spin-valley coupled optical selection rules: two exciton transitions—A and B—with opposite spins at the K/K' points couple selectively to light of opposite circular polarization, σ_{\pm} (Figure 1a).^{9,14-19} This optically addressable valley degree of freedom is the foundation for TMD-based 'valleytronics' which aims to realize next-generation computation and information processing technologies.^{10,20}

Valleytronic applications rely on long (\sim nanoseconds or greater) valley lifetimes, where the carrier imbalance created by selectively pumping K or K' lasts long enough for gate operations to be performed.^{10, 20} However, ultrafast sub- to few-picosecond valley depolarization²¹⁻²⁵ has been shown to occur through numerous mechanisms,^{26, 27} including the intervalley electron-hole exchange interaction,²⁸⁻³¹ intervalley scattering by defects³² or phonons,^{33, 34} and coupling to optically dark excitons.³⁵⁻³⁷ On the other hand, the valley lifetime of resident charge carriers is on the order of tens of picoseconds to nanoseconds,³⁸⁻⁴⁵ and nanosecond and microsecond polarization lifetimes have been measured for defect-bound excitons,⁴⁶ optically dark excitons,⁴⁷ and holes and interlayer excitons in stacked heterostructures.⁴⁸⁻⁵⁰

In addition to these dynamic valley depolarization mechanisms, immediate Coulomb-induced intervalley exciton coupling⁵¹ poses an additional exciton valley coupling channel. Dexter-like intervalley coupling,^{52, 53} intervalley renormalization,⁵⁴ and multi-exciton effects⁵⁵⁻⁵⁹ have been proposed to explain immediate intervalley coupling signatures observed in ultrafast transient absorption experiments. However, it is difficult to experimentally probe and differentiate the microscopic coupling mechanisms responsible for the initial ultrafast exciton valley depolarization or intervalley coupling with sub-100 fs resolution. Furthermore, the associated many-body interactions and resulting overlapping spectral signatures complicate the interpretation of ultrafast experiments at short time delays. Because optically bright excitons in TMD monolayers dominate the sub-picosecond optical response and the first stages of valley depolarization, they provide a key insight into the fundamental many-body interactions and microscopic couplings that limit the practical realization of valleytronics.⁶⁰

Here, we employ broadband helicity-resolved two-dimensional electronic spectroscopy (2DES) to map the ultrafast valley dynamics of A and B excitons in large-area monolayer MoS₂ films⁶¹ with \sim 10 fs temporal resolution (Figure 1b). We leverage the combined excitation-frequency and femtosecond resolution afforded by 2DES to determine whether resonant intervalley coupling (between A-A' or B-B' exciton states) and non-resonant intervalley coupling (between A-B' or B-A' exciton states) occurs together or on distinct timescales. We show strong experimental evidence for excitation fluence- and

temperature-independent intervalley coupling between all A and B valley exciton states on the sub-10 fs timescale. This coupling points to a single-particle mechanism separate from carrier-scattering or phonon-driven processes. These features persist in samples of differing grain size and inherent strain from the growth process, indicating ultrafast intervalley coupling on the timescale of excitation may be an intrinsic property of large-area TMD films. Our observations are not completely described by current theoretical frameworks, including multi-exciton effects or other Coulomb-induced coupling mechanisms. Elucidating the fundamental excitonic interactions that dominate the optical response and drive the initial valley dynamics in TMDs is critical to advancing valleytronic technologies.

RESULTS AND DISCUSSION

Monolayer MoS₂ films were prepared using a MOCVD growth procedure described previously,⁶¹ yielding wafer-scale continuous samples with $\sim \mu\text{m}$ grain sizes. Room-temperature linear absorption (Figure 1a) shows two peaks corresponding to the A and B excitons. To disentangle the ultrafast valley dynamics and couplings of the A and B excitons, we employ broadband helicity-resolved 2DES. Two-dimensional spectroscopy is an ultrafast four-wave mixing technique that correlates the excitation and detection frequencies of a system as a function of its ultrafast time evolution during the waiting time, T . By controlling the relative circular polarizations of the excitation and probe pulses in the 2DES experiments, we selectively probe intra- or intervalley dynamics and couplings with ~ 10 fs temporal resolution while maintaining knowledge of the excitation frequency. Importantly, 2DES allows us to measure correlations both between energetically resonant (A-A^(\dagger), B-B^(\dagger)) and non-resonant (A-B^(\dagger), B-A^(\dagger)) exciton states with valley resolution on the femtosecond timescale.

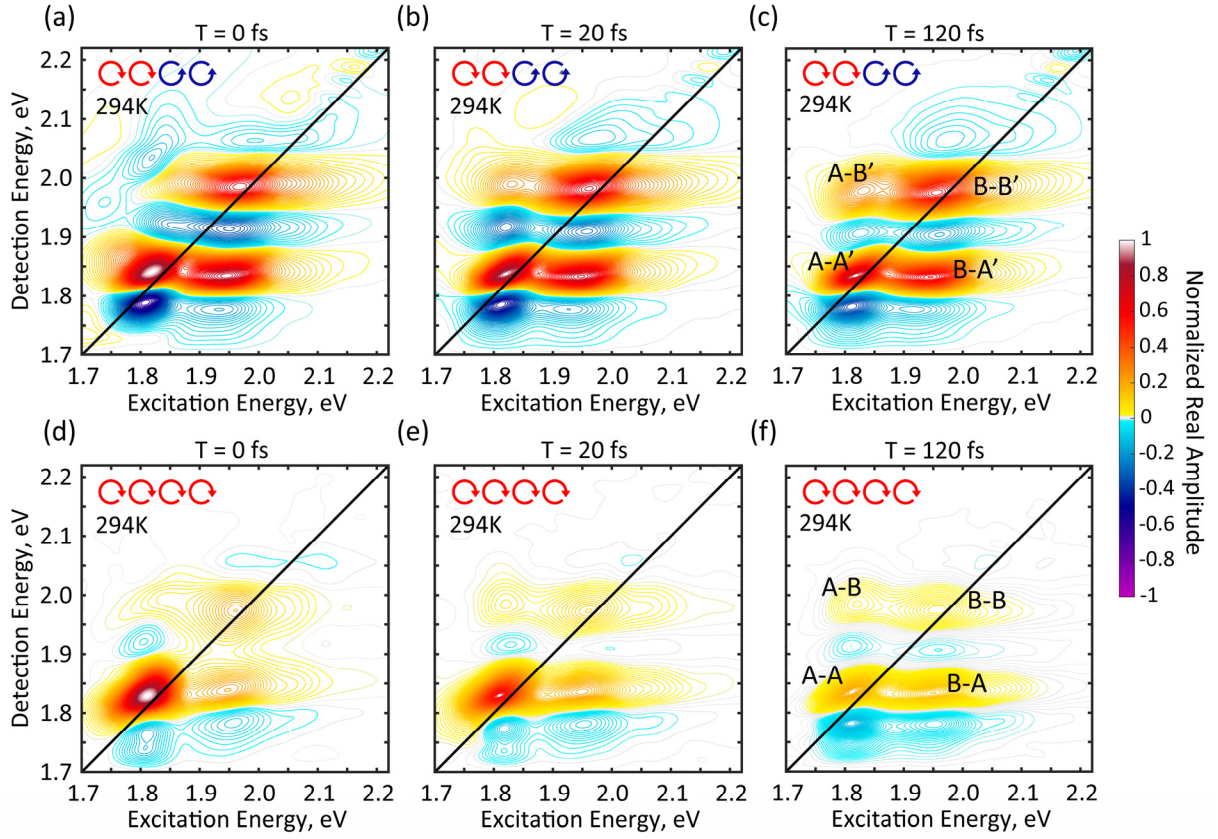


Figure 2. 2DES absorptive maps for cross- (a-c) and co- (d-f) circularly polarized pulse sequences at 294K for waiting times $T = 0, 20,$ and 120 fs. Cross-polarized spectra report on intervalley couplings while co-polarized spectra report on intravalley couplings. Main features of interest are annotated in the $T = 120$ fs frames, showing coupling between all A and B exciton states. Panels are normalized to the global maximum of the dataset, which is an average of $n = 8$ and $n = 3$ datasets for cross- and co-circularly polarized experiments, respectively. Spectra shown were acquired with an estimated carrier density of 1.4×10^{12} carriers/cm².

Room-temperature (294K) absorptive 2D spectra of MOCVD-grown monolayer MoS₂ at $T = 0,$ 20, and 120 fs are shown in Figure 2. In cross-circularly polarized experiments (Figure 2a-c), the detection event is in the opposite valley as excitation, whereas in co-polarized experiments (Figure 2d-f), the detection event is in the same valley as excitation. Therefore, cross- and co-polarized experiments probe inter- and intravalley dynamics and couplings, respectively. The spectra in Figure 2 were acquired with pulse energies of 3.5 nJ/pulse, corresponding to an estimated carrier density of 1.4×10^{12} carriers/cm² (See Supporting Information). Positive features correspond to ground state bleach and stimulated emission signals. Negative features correspond to photo-induced absorption (PIA) signals.

Two main peaks are prominent on the diagonal, in which the excitation and detection energies are equal, corresponding to the A and B excitons. Off-diagonal cross-peaks, where excitation and detection energies differ, correspond to coupling or energy transfer between the exciton states. For example, the lower cross-peak B-A' in the cross-polarized spectra corresponds to intervalley coupling through the excitation of B in one valley and detection of A' in the other valley. These main features are annotated in the $T = 120$ fs frames in Figure 2c and 2f. Additional 2D spectra are displayed in the Supporting Information.

The presence of significant signal strength in the cross-polarized spectra at short waiting time delays (Figure 2a-c), including $T = 0$ fs, is indicative of intervalley coupling processes on the timescale of pulsed optical excitation with sub-10 fs pulses (See Supporting Information for an estimation of the instrument response function). Importantly, bleaching, for example, of the K' transition after excitation at K, or *vice versa*, is not expected if the transitions are uncoupled (See Supporting Information). The cross-polarized spectra reveal strong intervalley coupling between non-resonant A and B excitons of the same spin (A-B', B-A') that appears as off-diagonal cross-peaks, and also between resonant excitons of opposite spin (A-A', B-B') that appears as diagonal features. Both resonant and non-resonant couplings appear with similar strength and timescale. In contrast, the co-polarized spectra are dominated primarily by a strong diagonal peak corresponding to the A exciton which quickly decays within tens of femtoseconds (Figure 2d-f). This concurrent ultrafast intravalley decay and intervalley signal appearance is consistent with a rapid intervalley population transfer.

We present normalized 2D spectra in Figure 2 to compare relative amplitudes of the spectral features within each experiment, highlighting that the intervalley coupling signatures appear with near-maximum amplitude on the timescale of optical excitation and are accompanied by fast decay of the intravalley features. Spectra normalized at late delay times (Figure S14) show that after the rapid initial intravalley decay, the relative intensities of the cross-peaks in both polarization sequences are comparable. Waiting time traces to ~ 1 ps (Figures S15, S16) show that differences in the intra- *versus* intervalley dynamics disappear nearly completely after ~ 100 fs; after this time, no further intervalley signal growth dynamics are observed, suggesting the valley coupling observed here occurs largely on the

timescale of excitation. Control experiments on the laser dye Nile Blue and a glass substrate show no appreciable difference between the polarization sequences (Figure S7, S8). Additionally, the spectral pattern of diagonal and off-diagonal cross-peaks persists to late delay times after $T = 0$ fs and has been reported previously in MoS₂.⁶² These observations indicate that the observed differences in MoS₂ originate from the valley-dependent material response and not, for example, polarization-dependent non-resonant or coherent artifacts.

Photo-induced absorption features redshifted in detection energy below the A exciton and between the A and B excitons are observed in both polarization sequences. The growth of the PIA feature below the diagonal A exciton peak in co-circularly polarized experiments is consistent with dynamic intravalley bandgap renormalization.⁶³⁻⁶⁶ The cross-peaks in the co-circularly polarized experiments arise from coupling between A and B excitons within the same valley. Guo *et al.*⁶² attribute these couplings to the intravalley exchange interaction using 2DES, while Wang *et al.*⁶⁷ describe intravalley spin-flip relaxation dynamics between the A and B excitons using two-color pump-probe measurements. Both of these studies report dynamic intravalley couplings on the sub- to few-hundred femtosecond timescale. Interestingly, the co-polarized spectra in Figure 2d-f show strong coupling cross-peaks at zero time delay, suggesting this intravalley coupling is enhanced in our measurements.

Immediate A-B' and B-A' intervalley coupling (as seen in Figure 2a, $T = 0$ fs) has previously been attributed to Dexter-like intervalley coupling between non-resonant excitons of the same spin in opposite valleys,^{52,53} and to intervalley renormalization *via* an intrinsic intervalley Coulombic coupling between A and B exciton states⁵⁴ in WS₂. Dexter-like intervalley coupling and intervalley renormalization mechanisms therefore provide a possible explanation for the observed A-B', B-A' coupling features in our cross-polarized experiments. Indeed, Dexter-like coupling efficiency may be enhanced in our experiments as the spin-orbit coupling of MoS₂ (~150meV) compared to WS₂ (~400meV) results in nearly three times greater Dexter-transfer efficiency.⁵² The fused silica substrate used in our experiments is predicted to further increase the Dexter transfer efficiency by ~15% compared to borosilicate used in previous studies.^{52,53} The relative intensity of the PIA features in the cross-polarized 2DES spectra is

stronger compared to the co-polarized 2DES spectra (Figure 2). This pattern is consistent with the intervalley renormalization process coupling A-B' and B'-A states,⁵⁴ which gives rise to characteristic dispersive lineshapes with pronounced redshifted PIA features. However, the most prominent dispersive character in our measurements is that of the A-A' diagonal feature, which is not coupled through the renormalization mechanism.

The A-A' and B-B' diagonal features, corresponding to intervalley coupling between energetically resonant exciton states of opposite spin. These diagonal features cannot be explained by Dexter-like and renormalization mechanisms which couple non-resonant excitons of the same spin in opposite valleys (B-A', A-B'). In contrast, the intervalley exchange interaction²⁸ leads to resonant intervalley coupling (A-A', B-B') *via* a simultaneous virtual exciton creation-annihilation process in opposite valleys. The intervalley exchange requires a non-zero exciton center-of-mass momentum, which may be created by disorder- or phonon-scattering, and has been widely implicated in sub- to few-picosecond valley depolarization. Both the Coulomb-induced intervalley renormalization and Dexter-like mechanism are predicted to dominate the 2nd-order impurity-driven intervalley exchange⁵⁴ on these short timescales,^{52, 53, 60} but we observe clear evidence that intervalley coupling between both resonant and non-resonant exciton states appear on similar ultrafast timescales during and after optical excitation (Figure 2).

To determine if the multiple intervalley coupling features seen in cross-polarized spectra may be driven by exciton-scattering or phonon-mediated mechanisms, we perform 2DES measurements at room-temperature (294K) at multiple excitation densities and at cryogenic temperature (6K). Waiting time traces for both polarization sequences of the A-A'(¹) diagonal features as well as the lower coupling B-A'(¹) cross-peaks are shown in Figure 3 at room-temperature for estimated carrier densities of 2.8×10^{12} , 1.4×10^{12} , and 5.6×10^{11} carriers/cm². The fluences used in these experiments are within the third-order regime⁶² and below the Mott density so that photo-excited electron-hole pairs primarily remain bound as excitons.^{68, 69}

The time traces probing the intervalley coupling (Figure 3a,b) are at a maximum at or shortly after $T = 0$ fs, similar to the estimated instrumental response function (Figures S5, S6). Interestingly,

while the below-diagonal B-A' intervalley cross-peaks are at a near-maximum within ~ 10 fs, the A-B' above-diagonal cross-peak features show growth dynamics on the ~ 20 fs timescale (Figure S19). We note that the data show a finite signal rise at negative delay times not captured by a transient grating experiment scanning T while $\tau = 0$ fs or reproduced by convolving a fit to the data with the instrument response function (Figures S23, S24). In addition to the finite pulse widths, signal at T < 0 fs will result from pulse-misordering artifacts leading to additional third-order signal pathways when scanning τ at T < 0 fs, or in the case of oscillations at T < 0 fs, dephasing.⁷⁰ We stress that despite the non-instantaneous response, the near-maximum signal amplitude at or shortly after T = 0 fs and lack of subsequent signal growth dynamics (Figure S15, S16) is strong evidence for ultrafast intervalley coupling during optical excitation.

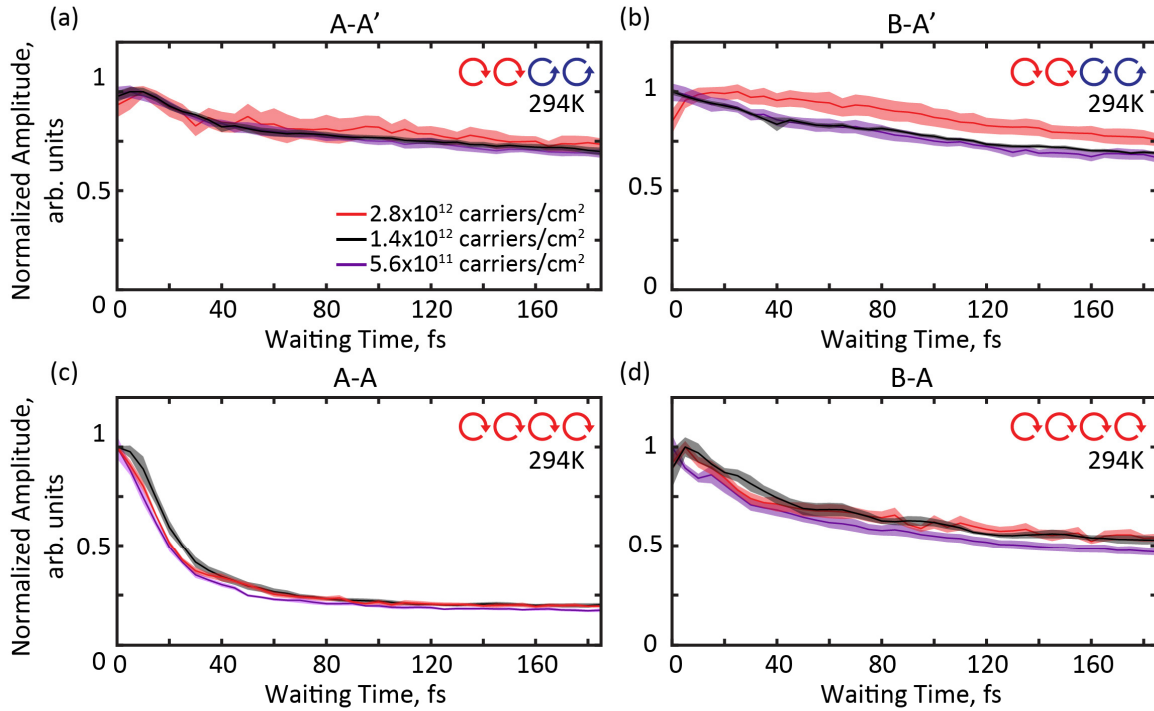


Figure 3. Room-temperature waiting time traces for cross- (a,b) and co- (c,d) circularly polarized pulse sequences at varying excitation fluences for the A-A^(*l*) diagonal and B-A^(*l*) lower cross-peak features. The data show minimal fluence-dependent dynamics within the error of the experiment. Each waiting time trace is normalized to the trace maximum. Shaded error bars represent the standard error of the mean averaging $n = 4$, $n = 8$, and $n = 6$ cross-polarized datasets and $n = 6$, $n = 3$, and $n = 5$ co-polarized datasets for fluences of 2.8×10^{12} , 1.4×10^{12} , and 5.6×10^{11} carriers/cm², respectively.

The data show no large fluence-dependent dynamics for these or other features in the spectra (Figure 3, S19, S22), ruling out exciton-exciton or carrier scattering as the dominant mechanism behind the ultrafast intervalley coupling on the sub-100 fs timescale. We also do not observe an appreciable fluence-dependence in the PIA features (See Supporting Information). In contrast, Schmidt *et al.*⁵⁴ observe a significant weakening of the intervalley PIA feature at excitation densities close to those in our measurements, and attribute this to the disorder-induced intervalley exchange interaction. We note that Mahmood *et al.*⁷¹ invoke an exciton-exciton two-particle exchange interaction to explain fluence-dependent valley depolarization dynamics on the few picosecond timescale in monolayer MoSe₂ and exciton-exciton annihilation has been shown at similar fluences on the tens of picosecond timescale in monolayer MoS₂.⁷² The sub-100 fs fluence-independent intervalley coupling in our work is therefore likely distinct from this exchange-mediated or other exciton scattering mechanisms. Kuhn *et al.*⁷³ observe fluence-independent ~170 fs intervalley depolarization (equal to the autocorrelation width of their 120 fs pulse) in monolayer MoSe₂ attributed to Rashba-induced mixing of dark and bright exciton states.⁷⁴ However, this coupling is predicted to be negligible in MoS₂⁷⁴ and is therefore likely not responsible for the observed coupling features in our experiments.

Cryogenic (6K) absolute value 2DES spectra (Figure 4) appear qualitatively similar to the room-temperature spectra (Figure S13). We observe a pattern of diagonal peaks and off-diagonal cross-peak features, and an increase in the relative strength of the spectral features in the cross-polarized spectra compared to the co-polarized spectra. While these absolute-value amplitude spectra cannot separate PIA from ground state bleach and stimulated emission signals, peaks in cross-polarized spectra remain indicative of intervalley coupling and transfer processes, and clear intervalley coupling features are observed at T = 0 fs at cryogenic temperature. The T = 0 fs spectrum (Figure 4a) appears to show two below-diagonal spectral features, while the later delay times show a single more intense lower cross-peak feature. While we cannot definitively assign an origin that explains this spectral pattern, we note that these absolute-value spectra contain purely dispersive contributions as well, including non-resonant response during the temporal pulse overlap at T = 0 fs. This effect, or an enhanced PIA feature, may

therefore be partially responsible for a change in peak shape or intensity in the short-time ($T = 0$ fs) 2D spectra. A comparison between cryogenic and room-temperature absolute-value spectra (Figure S13) show similar below diagonal B-A' spectral regions with a single prominent cross-peak at increased delay times.

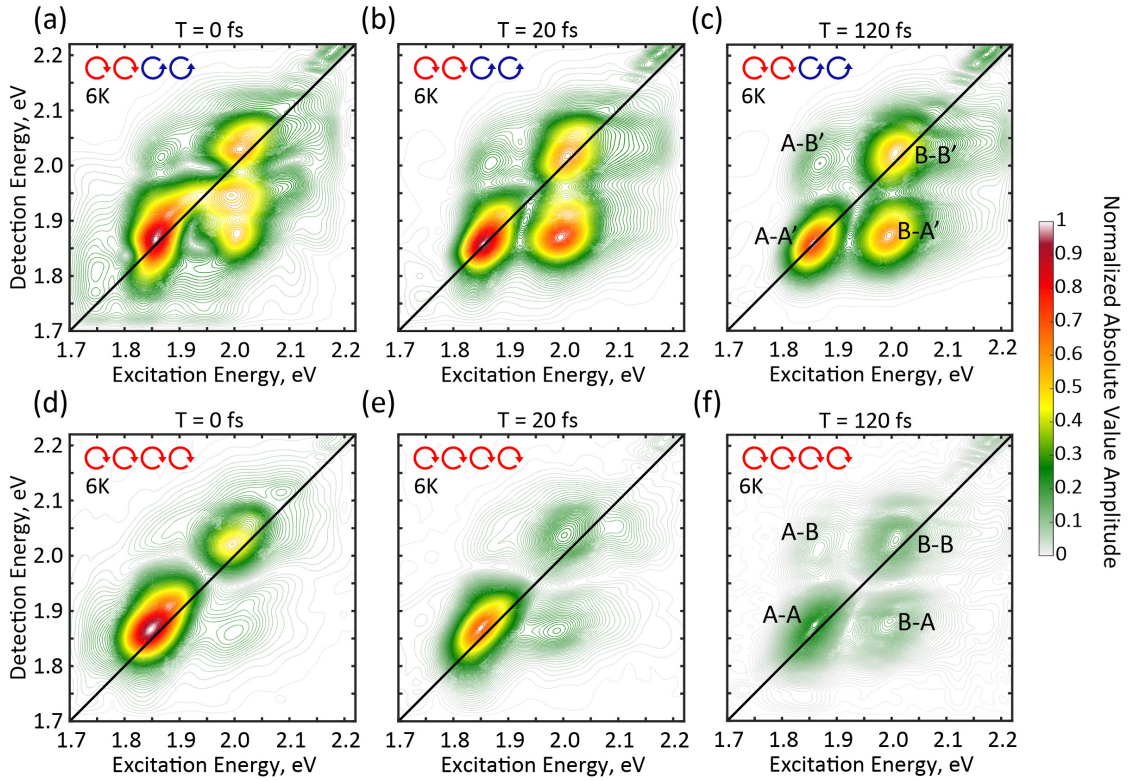


Figure 4. 2DES absolute-value amplitude maps for cross- (a-c) and co- (d-f) circularly polarized pulse sequences acquired at 6K and an estimated carrier density of 2.8×10^{12} carriers/cm². Similar to the room-temperature experiments in Figure 2, strong signal is observed in the opposite valley to excitation in the cross-polarized spectra accompanied by a fast decay of the co-polarized signal. Panels are normalized to the global maximum of the dataset, which is an average of $n = 6$, $n = 4$ datasets for the cross- and co-circularly polarized experiments, respectively.

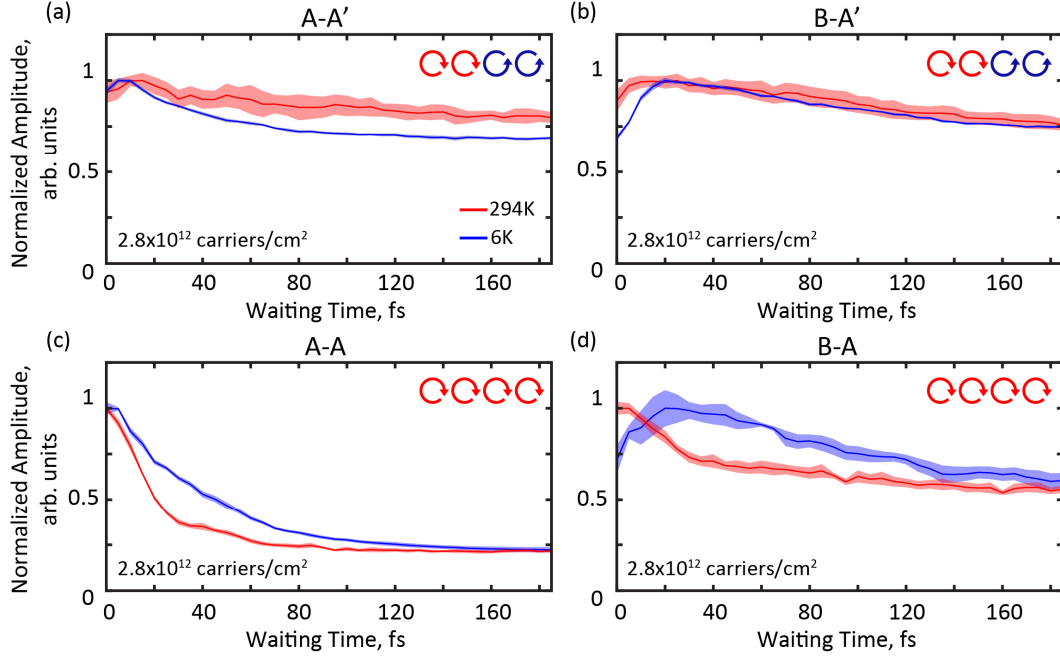


Figure 5. Waiting time traces for the A-A^(*i*) diagonal and B-A^(*i*) cross-peak features for both cross- and co-polarized pulse sequences at 6K and room-temperature and at a carrier density of 2.8×10^{12} carriers/cm². The cross-polarized intervalley dynamics show minimal temperature dependence whereas the co-polarized intravalley dynamics show a slower decay of the A exciton feature as well as a growth of the B to A cross-peak feature at cryogenic temperature. Each waiting time trace is normalized to the trace maximum. Shaded error bars represent the standard error of the mean averaging $n = 4$, $n = 6$ cross-polarized datasets and $n = 6$, $n = 4$ co-polarized datasets at room- and cryogenic temperature, respectively. Absolute-value data are shown.

The subsequent cross-polarized dynamics after $T = 0$ fs are relatively unchanged between room-temperature and 6K cryogenic experiments at the same excitation density (2.8×10^{12} carriers/cm²), shown in Figure 5 and Figure S20. This lack of temperature dependence indicates that it is unlikely that a phonon-driven process requiring thermally populated phonons plays a primary role in the observed intervalley coupling on this timescale. Phonon-mediated processes have been implicated previously in sub-picosecond intervalley scattering,³³ as well as exciton formation on the ~ 30 fs timescale⁷⁵ and interlayer charge separation in TMD heterostructures.⁷⁶ Nonadiabatic coupling of excitons to phonons has also been shown to couple exciton states, although this effect is suppressed in MoS₂ due to the large spin-orbit coupling compared to, for example, hexagonal boron nitride.⁷⁷ Phonon emission remains possible at cryogenic temperature, for example in intervalley scattering *via* the emission of acoustic phonons.⁷⁸ This

mechanism requires an excess above-bandgap excitation of twice the phonon energy.⁷⁹ However, we observe intervalley coupling across the entire spectral feature in our work, including at excitation of the exciton transitions, and not only after a threshold excitation energy. Interestingly, there is a temperature dependence in the co-polarized experiments probing the intravalley dynamics (Figure 5, lower panels). The B-A lower cross-peak shows a slower ~ 20 fs build-up at cryogenic temperature compared to room-temperature accompanied by a slightly slower decay of the A exciton diagonal feature, in line with previously described dynamic intravalley phonon-driven spin-flip or intravalley exchange mechanisms.^{62, 67} In addition, oscillations observed in the dynamics of the above-diagonal A-B cross-peak at cryogenic temperature (Figure S20d) may be evidence of intravalley coherence between the A and B excitons.

Intervalley PIA features in ultrafast transient absorption^{57-59, 80} and intervalley coupling cross-peaks in two-dimensional spectroscopy⁵⁵ experiments at short time delays have previously been attributed to intervalley multi-exciton effects. Indeed, exciton-exciton continua scattering and biexciton correlations are predicted to dominate the short time ($T = 0$ fs) transient absorption spectra of MoS₂ compared to other intervalley coupling mechanisms, including Dexter-like coupling, intervalley renormalization, and the intervalley exchange interaction, at cryogenic temperature (4K).⁵⁶ Katsch *et al.*⁵⁶ show blue-shifted intravalley PIA features in co-polarized experiments for both the A-A and B-B spectral features when including multiple Coulomb contributions, and redshifted intravalley PIA features enhanced in relative strength compared to intervalley PIA features when only considering exciton-exciton scattering and biexciton contributions. Although our cryogenic absolute-value spectra (Figure 4) cannot distinguish negative PIA features from positive bleach or stimulated emission features, our room-temperature spectra reveal distinctly stronger relative PIA features, including PIA features redshifted below the A exciton, in the cross-polarized compared to the co-polarized spectra (Figure 2). Furthermore, we expect features arising from biexciton coupling to be more pronounced at cryogenic temperature and higher excitation density, but our room- and cryogenic-temperature spectra appear qualitatively similar (Figures 2, 4, S13) and exhibit minimal fluence-dependence at room-temperature (Figure 3, Figures S10-S12). Additionally, previous work employing linearly polarized excitation in 2DES experiments observed weaker redshifted

PIA features at zero time delay at cryogenic temperature compared to room-temperature that dynamically increased in magnitude on the sub-100 fs timescale, providing evidence that bandgap renormalization dominated over biexciton formation.⁶³ Collectively, these observations suggest that direct optically induced biexciton formation is also likely not responsible for the intervalley coupling features observed in our measurements on large-area samples with increased disorder.

Charged exciton, or trion, resonances may also contribute to the coupling features observed in the 2DES spectra. Recent work has demonstrated sub-picosecond trion formation,⁸¹ coherent and incoherent exciton-trion coupling,⁸²⁻⁸⁴ and increased trion valley polarization lifetimes.^{22, 85} While the broad spectral features in our work preclude observing a possible distinct trion resonance,⁸⁶ intervalley coupling signatures are observed largely across entire spectral features whereas trion-mediated coupling would appear dominantly at either red-shifted excitation and detection energies from the main exciton peak, such as the A-A^(*v*) feature. For these reasons, the intervalley coupling signatures observed in our work likely do not originate from exciton-trion or trion-trion valley coupling.

Wafer-scale monolayer TMDs are attractive for technological applications; therefore, understanding the valley depolarization in these materials is of practical importance. Our experiments were performed on wafer (centimeter)-scale, MOCVD-grown monolayer films grown directly onto a fused silica substrate. These samples typically have a larger defect density compared to exfoliated samples, and the laser spot size used in our experiments ($\sim 290 \mu\text{m}$) illuminates many grains and grain boundaries ($\sim 1 \mu\text{m}$). Sample-to-sample as well as within-sample spatial variation of photoluminescence intensity or valley polarization values are well documented to be dependent on, for example, carrier doping,⁸⁷⁻⁸⁹ defect density⁹⁰⁻⁹² and strain.⁹³ However, these variations are often attributed to a dynamic competition between effective exciton lifetime and intervalley scattering time,¹⁴ whereas we observe coupling likely distinct from dynamic scattering mechanisms or non-radiative recombination.⁹⁴

To test whether the grain size or intrinsic strain from the growth process is responsible for the observed ultrafast intervalley coupling features, we performed helicity-resolved 2DES measurements at room-temperature on additional sample growths with different grain sizes ($\sim 2 \mu\text{m}$ and $\sim 0.2 \mu\text{m}$). These

samples were transferred from their original growth substrates to a clean fused silica substrate using a dry, vacuum-transfer process⁹⁵ to relieve any strain present in the as-grown films (see Figures S1, S2 for absorption and photoluminescence data confirming the strain release through an increase in the bandgap of the transferred samples). The 2DES spectra of these samples show qualitatively similar spectral features at short time delay (Figures S25, S26), indicating the effects of grain size, intrinsic strain from the growth process, or sample variation are likely not directly responsible for the observed intervalley coupling.

Defects, or other properties, of large-area samples may facilitate direct valley coupling shortly after excitation or change the relative strength, timescales, or interplay of the existing mechanisms that are currently inconsistent with our observations.²⁷ For example, enhanced intravalley exchange mixing of A and B excitons within one valley may facilitate intervalley coupling among all A and B exciton states through the intervalley exchange, Dexter-like coupling, or renormalization on similar ultrafast timescales. The co-polarized 2DES spectra in this work (Figures 2, 4) show prominent intravalley coupling cross-peaks at short delay, including $T = 0$ fs, suggesting the intravalley exchange may indeed be enhanced in these large-area samples. Interestingly, previous work suggests that defects may be used to enhance the robustness of the valley index⁴⁶ and that some defect types such as sulfur vacancies in MoS₂ may protect against intervalley scattering.⁹⁶ Future experimental and theoretical investigation is therefore required to determine the degree to which the relative strength and timescale of the ultrafast intervalley coupling depends on these intrinsic or extrinsic sample factors such as dielectric environment, strain, grain boundaries, and defect density, and to separate fundamental changes in static electronic structure from those giving rise to dynamic scattering or coupling processes.

CONCLUSIONS

Employing broadband helicity-resolved 2DES, we have provided strong experimental evidence for intervalley exciton coupling between all A and B valley exciton states on the ~ 10 fs timescale in large-area, MOCVD-grown monolayer MoS₂. These couplings lead to a complete loss of the differences in

intra- *versus* intervalley dynamics within ~ 100 fs (Figure S15, S16). In particular, the simultaneous appearance of resonant (A-A', B-B') and non-resonant (A-B', B-A') intervalley coupling features and the lack of fluence- or temperature-dependent dynamics preclude attributing our observations to widely discussed intervalley coupling mechanisms, including the intervalley exchange interaction and multiexciton effects. The intervalley couplings observed in our work are robust to sample grain size and inherent strain from the growth process, and therefore may be a characteristic feature of large-area samples. This coupling therefore poses a fundamental challenge to exploiting optically bright single excitons in TMD-based valleytronic applications that require a robust valley index.

METHODS

The monolayer MoS₂ films were grown using metal-organic chemical vapor deposition in a home-built hot-walled, horizontal tube furnace according to the procedures described by Kang *et al.*⁶¹ Substrates for the growth were either fused SiO₂ wafers or Si wafers with 300 nm thermal SiO₂. The films grown on Si wafers were transferred to fused SiO₂ after the growth using a dry, vacuum transfer process according to the process outlined in Kang *et al.*⁹⁵ SEM measurements were performed on a Zeiss Merlin Field-Emission Scanning Electron Microscope using secondary-electron imaging at accelerating voltages between 1-3 kV. Raman and PL spectra were acquired using a Horiba LabRamHR Evolution confocal Raman microscope with a 532 nm excitation.

Two-dimensional spectroscopic experiments were performed using a setup described previously.⁹⁷ Briefly, a Ti:Sapphire modelocked oscillator (Coherent, Inc.) operating at an 80 MHz repetition rate seeds a Ti:Sapphire regenerative amplifier (Coherent, Inc.) to produce a 5 kHz pulse train of ~ 38 fs pulse width centered around 800 nm. Subsequent filamentation in a 2 m tube of Argon held at ~ 16 psig broadens the spectrum to cover ~ 400 to 900 nm. An angle-tunable dichroic filter spectrally truncates the output, rejecting light red of 730 nm. The resulting white-light pulses are compressed *via* a chirped mirror pair and a pulse shaper (MIIPS, Biophotonics, Inc.) to ~ 8 fs. The spectrum is also shaped

with an amplitude mask by the MIIPS pulse shaper, producing an excitation spectrum without strong wavelength dependence.

The all-reflective two-dimensional interferometer produces interpulse delays in the coherence time, τ , with a resolution of ~ 20 as using angle mechanical stepper motor stages (Aerotech Inc.) without introducing additional dispersion. Four pulses aligned to the four corners of a box are focused to a spot of $\sim 290 \mu\text{m}$ on the sample by a 750 mm spherical mirror. Interaction of pulses 1, 2, and 3 generate a third-order nonlinear signal, while a fourth pulse attenuated by a factor of $\sim 10^5$ is used as a local oscillator in heterodyne detection. The resulting heterodyned signal is spectrally dispersed *via* a spectrometer (Shamrock) onto a CCD array camera (Andor Newton EM).

Broadband half-waveplates (Union Optic) in the path of each beam control the relative linear polarization to be either all co-linear or cross-linear pulse polarization such that beams 3 and 4 have orthogonal linear polarization to beams 1 and 2. A single broadband quarter-waveplate directly before the sample position produces co- or cross-circularly polarized sequences depending on the initial linear polarization. Circular polarization purity of $\sim 90\%$ is achieved for all beams in the described experiments as measured by the combination of a Glan-Thompson polarizer and power meter (see Supporting Information).

Two-dimensional spectra were acquired by stepping τ from -90 fs to 90 fs in 1.5 fs steps for a given waiting time, T . Hann, 75% Tukey, and Nuttall windows are used in apodization during data processing in the rephasing time (t), coherence time (τ), and waiting time frequency (ω_T) domains, respectively, in combination with static scatter subtraction using mechanical shutters to remove beam scatter and other unwanted signals.⁹⁸ Fully absorptive, real-valued spectra were obtained by phasing according to the projection-slice theorem^{99, 100} after acquiring separate pump-probe measurements with matched excitation fluences. Changing experimental setups and avoiding a warm-up of the sample precluded acquiring cryogenic pump-probe measurements of the same sample, and absolute-value 2DES data are shown for cryogenic experiments. These spectra therefore contain both purely absorptive and dispersive contributions.

ASSOCIATED CONTENT

Supporting Information

The Supporting Information is available free of charge at <https://pubs.acs.org>.

Monolayer MoS₂ characterization (UV-Vis, photoluminescence, and Raman spectra and SEM image), and femtosecond pulse characterization used in 2DES experiments. Additional 2DES spectra and waiting time traces, 2DES spectra of strain-relieved samples, and excitation fluence calculations. Discussion of coupling cross-peaks in 2D spectroscopy.

Financial Interest Statement

The authors declare no competing financial interest.

AUTHOR INFORMATION

Corresponding Author

*Email: gsengel@uchicago.edu

Author Contributions

L.T.L., R.E.W., F.M., S.S., J.P., and G.S.E. designed the research. L.T.L., R.E.W., and S.S. performed the 2DES measurements with assistance from P-C.T. and K.L.J. F.M. synthesized and characterized the MoS₂ samples. L.T.L. and R.E.W. processed the experimental data. All authors discussed the experimental findings and interpreted the results. L.T.L. wrote the manuscript with input from all authors.

ACKNOWLEDGEMENTS

The authors thank Dr. Karen M. Watters for scientific editing and Christopher Melnychuk for helpful discussions. This work was supported by the Air Force Office of Scientific Research (AFOSR) (FA9550-18-1-0099) and the NSF (under grant no. 1900359). This work was also supported by the NSF MRSEC

grant program at the University of Chicago (DMR-1420709 and DMR-2011854). F.M. and J.S.H. acknowledge support from the NSF-GRFP program under grant no. DGE-1746045. R.E.W. acknowledges support from the National Defense Science & Engineering Graduate Fellowship (NDSEG) Program, 32 CFR 168a, funded through the AFOSR and the Department of Defense. The MoS₂ visualization in Figure 1b was produced using the VESTA software.¹⁰¹

REFERENCES

1. Jariwala, D.; Sangwan, V. K.; Lauhon, L. J.; Marks, T. J.; Hersam, M. C., Emerging Device Applications for Semiconducting Two-Dimensional Transition Metal Dichalcogenides. *ACS Nano* **2014**, *8*, 1102-1120.
2. Mak, K. F.; Shan, J., Photonics and Optoelectronics of 2D Semiconductor Transition Metal Dichalcogenides. *Nat. Photonics* **2016**, *10*, 216-226.
3. Mueller, T.; Malic, E., Exciton Physics and Device Application of Two-Dimensional Transition Metal Dichalcogenide Semiconductors. *npj 2D Mater. Appl.* **2018**, *2*, 29.
4. Mak, K. F.; Lee, C.; Hone, J.; Shan, J.; Heinz, T. F., Atomically Thin MoS₂: A New Direct-Gap Semiconductor. *Phys. Rev. Lett.* **2010**, *105*, 136805.
5. Splendiani, A.; Sun, L.; Zhang, Y.; Li, T.; Kim, J.; Chim, C. Y.; Galli, G.; Wang, F., Emerging Photoluminescence in Monolayer MoS₂. *Nano Lett.* **2010**, *10*, 1271-1275.
6. Qiu, D. Y.; da Jornada, F. H.; Louie, S. G., Optical Spectrum of MoS₂: Many-Body Effects and Diversity of Exciton States. *Phys. Rev. Lett.* **2013**, *111*, 216805.
7. Chernikov, A.; Berkelbach, T. C.; Hill, H. M.; Rigosi, A.; Li, Y.; Aslan, O. B.; Reichman, D. R.; Hybertsen, M. S.; Heinz, T. F., Exciton Binding Energy and Nonhydrogenic Rydberg Series in Monolayer WS₂. *Phys. Rev. Lett.* **2014**, *113*, 076802.
8. Cho, Y.; Berkelbach, T. C., Environmentally Sensitive Theory of Electronic and Optical Transitions in Atomically Thin Semiconductors. *Phys. Rev. B* **2018**, *97*, 041409.
9. Yao, W.; Xiao, D.; Niu, Q., Valley-Dependent Optoelectronics from Inversion Symmetry Breaking. *Phys. Rev. B* **2008**, *77*, 235406.
10. Schaibley, J. R.; Yu, H.; Clark, G.; Rivera, P.; Ross, J. S.; Seyler, K. L.; Yao, W.; Xu, X., Valleytronics in 2D Materials. *Nat. Rev. Mater.* **2016**, *1*, 16055.
11. Mak, K. F.; He, K.; Lee, C.; Lee, G. H.; Hone, J.; Heinz, T. F.; Shan, J., Tightly Bound Trions in Monolayer MoS₂. *Nat. Mater.* **2013**, *12*, 207-211.

12. Plechinger, G.; Nagler, P.; Kraus, J.; Paradiso, N.; Strunk, C.; Schüller, C.; Korn, T., Identification of Excitons, Trions and Biexcitons in Single-Layer WS₂. *Phys. Status Solidi RRL* **2015**, *9*, 457-461.
13. You, Y.; Zhang, X.-X.; Berkelbach, T. C.; Hybertsen, M. S.; Reichman, D. R.; Heinz, T. F., Observation of Biexcitons in Monolayer WSe₂. *Nat. Phys.* **2015**, *11*, 477-481.
14. Mak, K. F.; He, K.; Shan, J.; Heinz, T. F., Control of Valley Polarization in Monolayer MoS₂ by Optical Helicity. *Nat. Nanotechnol.* **2012**, *7*, 494-498.
15. Xiao, D.; Liu, G. B.; Feng, W.; Xu, X.; Yao, W., Coupled Spin and Valley Physics in Monolayers of MoS₂ and Other Group-VI Dichalcogenides. *Phys. Rev. Lett.* **2012**, *108*, 196802.
16. Zeng, H.; Dai, J.; Yao, W.; Xiao, D.; Cui, X., Valley Polarization in MoS₂ Monolayers by Optical Pumping. *Nat. Nanotechnol.* **2012**, *7*, 490-493.
17. Cao, T.; Wang, G.; Han, W.; Ye, H.; Zhu, C.; Shi, J.; Niu, Q.; Tan, P.; Wang, E.; Liu, B.; Feng, J., Valley-Selective Circular Dichroism of Monolayer Molybdenum Disulfide. *Nat. Commun.* **2012**, *3*, 887.
18. Xu, X.; Yao, W.; Xiao, D.; Heinz, T. F., Spin and Pseudospins in Layered Transition Metal Dichalcogenides. *Nat. Phys.* **2014**, *10*, 343-350.
19. Mak, K. F.; Xiao, D.; Shan, J., Light-Valley Interactions in 2D Semiconductors. *Nat. Photonics* **2018**, *12*, 451-460.
20. Vitale, S. A.; Nezich, D.; Varghese, J. O.; Kim, P.; Gedik, N.; Jarillo-Herrero, P.; Xiao, D.; Rothschild, M., Valleytronics: Opportunities, Challenges, and Paths Forward. *Small* **2018**, *14*, e1801483.
21. Mai, C.; Semenov, Y. G.; Barrette, A.; Yu, Y.; Jin, Z.; Cao, L.; Kim, K. W.; Gundogdu, K., Exciton Valley Relaxation in a Single Layer of WS₂ Measured by Ultrafast Spectroscopy. *Phys. Rev. B* **2014**, *90*, 041414.
22. Hao, K.; Xu, L.; Wu, F.; Nagler, P.; Tran, K.; Ma, X.; Schuller, C.; Korn, T.; MacDonald, A. H.; Moody, G.; Li, X., Trion Valley Coherence in Monolayer Semiconductors. *2D Mater.* **2017**, *4*, 025105.
23. Dal Conte, S.; Bottegoni, F.; Pogna, E. A. A.; De Fazio, D.; Ambrogio, S.; Bargigia, I.; D'Andrea, C.; Lombardo, A.; Bruna, M.; Ciccacci, F.; Ferrari, A. C.; Cerullo, G.; Finazzi, M., Ultrafast Valley Relaxation Dynamics in Monolayer MoS₂ Probed by Nonequilibrium Optical Techniques. *Phys. Rev. B* **2015**, *92*, 235425.
24. Moody, G.; Schaibley, J.; Xu, X., Exciton Dynamics in Monolayer Transition Metal Dichalcogenides. *J. Opt. Soc. Am. B* **2016**, *33*, C39-C49.
25. Plechinger, G.; Nagler, P.; Arora, A.; Schmidt, R.; Chernikov, A.; Del Aguila, A. G.; Christianen, P. C.; Bratschitsch, R.; Schuller, C.; Korn, T., Trion Fine Structure and Coupled Spin-Valley Dynamics in Monolayer Tungsten Disulfide. *Nat. Commun.* **2016**, *7*, 12715.

26. Selig, M.; Katsch, F.; Schmidt, R.; Michaelis de Vasconcellos, S.; Bratschitsch, R.; Malic, E.; Knorr, A., Ultrafast Dynamics in Monolayer Transition Metal Dichalcogenides: Interplay of Dark Excitons, Phonons, and Intervalley Exchange. *Phys. Rev. Res.* **2019**, *1*, 022007.
27. Jiang, X.; Zheng, Q.; Lan, Z.; Saidi, W. A.; Ren, X.; Zhao, J., Real-Time *GW*-BSE Investigations on Spin-Valley Exciton Dynamics in Monolayer Transition Metal Dichalcogenide. *Sci. Adv.* **2021**, *7*, eabf3759.
28. Yu, T.; Wu, M. W., Valley Depolarization Due to Intervalley and Intravalley Electron-Hole Exchange Interactions in Monolayer MoS₂. *Phys. Rev. B* **2014**, *89*, 205303.
29. Glazov, M. M.; Amand, T.; Marie, X.; Lagarde, D.; Bouet, L.; Urbaszek, B., Exciton Fine Structure and Spin Decoherence in Monolayers of Transition Metal Dichalcogenides. *Phys. Rev. B* **2014**, *89*, 201302.
30. Yu, H.; Liu, G. B.; Gong, P.; Xu, X.; Yao, W., Dirac Cones and Dirac Saddle Points of Bright Excitons in Monolayer Transition Metal Dichalcogenides. *Nat. Commun.* **2014**, *5*, 3876.
31. Maialle, M. Z.; de Andrada e Silva, E. A.; Sham, L. J., Exciton Spin Dynamics in Quantum Wells. *Phys. Rev. B Condens. Matter* **1993**, *47*, 15776-15788.
32. Wang, Q.; Ge, S.; Li, X.; Qiu, J.; Ji, Y.; Feng, J.; Sun, D., Valley Carrier Dynamics in Monolayer Molybdenum Disulfide from Helicity-Resolved Ultrafast Pump-Probe Spectroscopy. *ACS Nano* **2013**, *7*, 11087-11093.
33. Molina-Sanchez, A.; Sangalli, D.; Wirtz, L.; Marini, A., *Ab Initio* Calculations of Ultrashort Carrier Dynamics in Two-Dimensional Materials: Valley Depolarization in Single-Layer WSe₂. *Nano Lett.* **2017**, *17*, 4549-4555.
34. Xu, S.; Si, C.; Li, Y.; Gu, B. L.; Duan, W., Valley Depolarization Dynamics in Monolayer Transition-Metal Dichalcogenides: Role of the Satellite Valley. *Nano Lett.* **2021**, *21*, 1785-1791.
35. Selig, M.; Katsch, F.; Brem, S.; Mkrtchian, G. F.; Malic, E.; Knorr, A., Suppression of Intervalley Exchange Coupling in the Presence of Momentum-Dark States in Transition Metal Dichalcogenides. *Phys. Rev. Res.* **2020**, *2*, 023322.
36. Selig, M.; Berghäuser, G.; Raja, A.; Nagler, P.; Schuller, C.; Heinz, T. F.; Korn, T.; Chernikov, A.; Malic, E.; Knorr, A., Excitonic Linewidth and Coherence Lifetime in Monolayer Transition Metal Dichalcogenides. *Nat. Commun.* **2016**, *7*, 13279.
37. Selig, M.; Berghäuser, G.; Richter, M.; Bratschitsch, R.; Knorr, A.; Malic, E., Dark and Bright Exciton Formation, Thermalization, and Photoluminescence in Monolayer Transition Metal Dichalcogenides. *2D Mater.* **2018**, *5*, 035017.
38. Lu, H. Z.; Yao, W.; Xiao, D.; Shen, S. Q., Intervalley Scattering and Localization Behaviors of Spin-Valley Coupled Dirac Fermions. *Phys. Rev. Lett.* **2013**, *110*, 016806.
39. Ochoa, H.; Roldán, R., Spin-Orbit-Mediated Spin Relaxation in Monolayer MoS₂. *Phys. Rev. B* **2013**, *87*, 245421.

40. Wang, L.; Wu, M. W., Electron Spin Relaxation Due to D'yakonov-Perel' and Elliot-Yafet Mechanisms in Monolayer MoS₂: Role of Intravalley and Intervalley Processes. *Phys. Rev. B* **2014**, *89*, 115302.
41. Wang, L.; Wu, M. W., Intrinsic Electron Spin Relaxation Due to the D'yakonov-Perel' Mechanism in Monolayer MoS₂. *Phys. Lett. A* **2014**, *378*, 1336-1340.
42. Yang, L.; Sinitsyn, N. A.; Chen, W.; Yuan, J.; Zhang, J.; Lou, J.; Crooker, S. A., Long-Lived Nanosecond Spin Relaxation and Spin Coherence of Electrons in Monolayer MoS₂ and WS₂. *Nat. Phys.* **2015**, *11*, 830-834.
43. Song, X.; Xie, S.; Kang, K.; Park, J.; Sih, V., Long-Lived Hole Spin/Valley Polarization Probed by Kerr Rotation in Monolayer WSe₂. *Nano Lett.* **2016**, *16*, 5010-5014.
44. Yan, T.; Yang, S.; Li, D.; Cui, X., Long Valley Relaxation Time of Free Carriers in Monolayer WSe₂. *Phys. Rev. B* **2017**, *95*, 241406.
45. Zhou, H.; Zhao, Y.; Tao, W.; Li, Y.; Zhou, Q.; Zhu, H., Controlling Exciton and Valley Dynamics in Two-Dimensional Heterostructures with Atomically Precise Interlayer Proximity. *ACS Nano* **2020**, *14*, 4618-4625.
46. Moody, G.; Tran, K.; Lu, X.; Autry, T.; Fraser, J. M.; Mirin, R. P.; Yang, L.; Li, X.; Silverman, K. L., Microsecond Valley Lifetime of Defect-Bound Excitons in Monolayer WSe₂. *Phys. Rev. Lett.* **2018**, *121*, 057403.
47. Tang, Y.; Mak, K. F.; Shan, J., Long Valley Lifetime of Dark Excitons in Single-Layer WSe₂. *Nat. Commun.* **2019**, *10*, 4047.
48. Rivera, P.; Seyler, K. L.; Yu, H.; Schaibley, J. R.; Yan, J.; Mandrus, D. G.; Yao, W.; Xu, X., Valley-Polarized Exciton Dynamics in a 2D Semiconductor Heterostructure. *Science* **2016**, *351*, 688.
49. Kim, J.; Jin, C.; Chen, B.; Cai, H.; Zhao, T.; Lee, P.; Kahn, S.; Watanabe, K.; Taniguchi, T.; Tongay, S.; Crommie, M. F.; Wang, F., Observation of Ultralong Valley Lifetime in WSe₂/MoS₂ Heterostructures. *Sci. Adv.* **2017**, *3*, e1700518.
50. Jiang, C.; Xu, W.; Rasmita, A.; Huang, Z.; Li, K.; Xiong, Q.; Gao, W. B., Microsecond Dark-Exciton Valley Polarization Memory in Two-Dimensional Heterostructures. *Nat. Commun.* **2018**, *9*, 753.
51. Katsch, F.; Selig, M.; Carmele, A.; Knorr, A., Theory of Exciton-Exciton Interactions in Monolayer Transition Metal Dichalcogenides. *Phys. Status Solidi B* **2018**, *255*, 1800185.
52. Berghäuser, G.; Bernal-Villamil, I.; Schmidt, R.; Schneider, R.; Niehues, I.; Erhart, P.; Michaelis de Vasconcellos, S.; Bratschitsch, R.; Knorr, A.; Malic, E., Inverted Valley Polarization in Optically Excited Transition Metal Dichalcogenides. *Nat. Commun.* **2018**, *9*, 971.
53. Bernal-Villamil, I.; Berghäuser, G.; Selig, M.; Niehues, I.; Schmidt, R.; Schneider, R.; Tonndorf, P.; Erhart, P.; de Vasconcellos, S. M.; Bratschitsch, R.; Knorr, A.; Malic, E., Exciton Broadening and Band Renormalization Due to Dexter-Like Intervalley Coupling. *2D Mater.* **2018**, *5*, 025011.

54. Schmidt, R.; Berghauser, G.; Schneider, R.; Selig, M.; Tonndorf, P.; Malic, E.; Knorr, A.; Michaelis de Vasconcellos, S.; Bratschitsch, R., Ultrafast Coulomb-Induced Intervalley Coupling in Atomically Thin WS₂. *Nano Lett.* **2016**, *16*, 2945-2950.
55. Hao, K.; Specht, J. F.; Nagler, P.; Xu, L.; Tran, K.; Singh, A.; Dass, C. K.; Schuller, C.; Korn, T.; Richter, M.; Knorr, A.; Li, X.; Moody, G., Neutral and Charged Inter-Valley Biexcitons in Monolayer MoSe₂. *Nat. Commun.* **2017**, *8*, 15552.
56. Katsch, F.; Selig, M.; Knorr, A., Theory of Coherent Pump-Probe Spectroscopy in Monolayer Transition Metal Dichalcogenides. *2D Mater.* **2019**, *7*, 015021.
57. Steinhoff, A.; Florian, M.; Singh, A.; Tran, K.; Kolarczik, M.; Helmrich, S.; Achtstein, A. W.; Woggon, U.; Owschimikow, N.; Jahnke, F.; Li, X., Biexciton Fine Structure in Monolayer Transition Metal Dichalcogenides. *Nat. Phys.* **2018**, *14*, 1199-1204.
58. Sie, E. J.; Frenzel, A. J.; Lee, Y.-H.; Kong, J.; Gedik, N., Intervalley Biexcitons and Many-Body Effects in Monolayer MoS₂. *Phys. Rev. B* **2015**, *92*, 125417.
59. Mai, C.; Barrette, A.; Yu, Y.; Semenov, Y. G.; Kim, K. W.; Cao, L.; Gundogdu, K., Many-Body Effects in Valleytronics: Direct Measurement of Valley Lifetimes in Single-Layer MoS₂. *Nano Lett.* **2014**, *14*, 202-206.
60. Dal Conte, S.; Trovatiello, C.; Gadermaier, C.; Cerullo, G., Ultrafast Photophysics of 2D Semiconductors and Related Heterostructures. *Trends Chem.* **2019**, *2*, 28-42.
61. Kang, K.; Xie, S.; Huang, L.; Han, Y.; Huang, P. Y.; Mak, K. F.; Kim, C. J.; Muller, D.; Park, J., High-Mobility Three-Atom-Thick Semiconducting Films with Wafer-Scale Homogeneity. *Nature* **2015**, *520*, 656-660.
62. Guo, L.; Wu, M.; Cao, T.; Monahan, D. M.; Lee, Y.-H.; Louie, S. G.; Fleming, G. R., Exchange-Driven Intravalley Mixing of Excitons in Monolayer Transition Metal Dichalcogenides. *Nat. Phys.* **2018**, *15*, 228-232.
63. Wood, R. E.; Lloyd, L. T.; Mujid, F.; Wang, L.; Allodi, M. A.; Gao, H.; Mazuski, R.; Ting, P. C.; Xie, S.; Park, J.; Engel, G. S., Evidence for the Dominance of Carrier-Induced Band Gap Renormalization over Biexciton Formation in Cryogenic Ultrafast Experiments on MoS₂ Monolayers. *J. Phys. Chem. Lett.* **2020**, *11*, 2658-2666.
64. Pogna, E. A.; Marsili, M.; De Fazio, D.; Dal Conte, S.; Manzoni, C.; Sangalli, D.; Yoon, D.; Lombardo, A.; Ferrari, A. C.; Marini, A.; Cerullo, G.; Prezzi, D., Photo-Induced Bandgap Renormalization Governs the Ultrafast Response of Single-Layer MoS₂. *ACS Nano* **2016**, *10*, 1182-1188.
65. Cunningham, P. D.; Hanbicki, A. T.; McCreary, K. M.; Jonker, B. T., Photoinduced Bandgap Renormalization and Exciton Binding Energy Reduction in WS₂. *ACS Nano* **2017**, *11*, 12601-12608.
66. Smejkal, V.; Libisch, F.; Molina-Sanchez, A.; Trovatiello, C.; Wirtz, L.; Marini, A., Time-Dependent Screening Explains the Ultrafast Excitonic Signal Rise in 2D Semiconductors. *ACS Nano* **2021**, *15*, 1179-1185.

67. Wang, Z.; Molina-Sanchez, A.; Altmann, P.; Sangalli, D.; De Fazio, D.; Soavi, G.; Sassi, U.; Bottegoni, F.; Ciccacci, F.; Finazzi, M.; Wirtz, L.; Ferrari, A. C.; Marini, A.; Cerullo, G.; Dal Conte, S., Intravalley Spin-Flip Relaxation Dynamics in Single-Layer WS₂. *Nano Lett.* **2018**, *18*, 6882-6891.
68. Chernikov, A.; Ruppert, C.; Hill, H. M.; Rigosi, A. F.; Heinz, T. F., Population Inversion and Giant Bandgap Renormalization in Atomically Thin WS₂ Layers. *Nat. Photonics* **2015**, *9*, 466-470.
69. Steinhoff, A.; Florian, M.; Rösner, M.; Schönhoff, G.; Wehling, T. O.; Jahnke, F., Exciton Fission in Monolayer Transition Metal Dichalcogenide Semiconductors. *Nat. Commun.* **2017**, *8*, 1166.
70. Richter, J. M.; Branchi, F.; Valduga de Almeida Camargo, F.; Zhao, B.; Friend, R. H.; Cerullo, G.; Deschler, F., Ultrafast Carrier Thermalization in Lead Iodide Perovskite Probed with Two-Dimensional Electronic Spectroscopy. *Nat. Commun.* **2017**, *8*, 376.
71. Mahmood, F.; Alpichshev, Z.; Lee, Y. H.; Kong, J.; Gedik, N., Observation of Exciton-Exciton Interaction Mediated Valley Depolarization in Monolayer MoSe₂. *Nano Lett.* **2018**, *18*, 223-228.
72. Sun, D.; Rao, Y.; Reider, G. A.; Chen, G.; You, Y.; Brezin, L.; Harutyunyan, A. R.; Heinz, T. F., Observation of Rapid Exciton-Exciton Annihilation in Monolayer Molybdenum Disulfide. *Nano Lett.* **2014**, *14*, 5625-5629.
73. Kuhn, H.; Wagner, J.; Han, S.; Bernhardt, R.; Gao, Y.; Xiao, L.; Zhu, J.; Loosdrecht, P. H. M., Excitonic Transport and Intervalley Scattering Dynamics in Large-Size Exfoliated MoSe₂ Monolayer Investigated by Heterodyned Transient Grating Spectroscopy. *Laser Photonics Rev.* **2020**, *14*, 2000029.
74. Yang, M.; Robert, C.; Lu, Z.; Van Tuan, D.; Smirnov, D.; Marie, X.; Dery, H., Exciton Valley Depolarization in Monolayer Transition-Metal Dichalcogenides. *Phys. Rev. B* **2020**, *101*, 115307.
75. Trovatiello, C.; Katsch, F.; Borys, N. J.; Selig, M.; Yao, K.; Borrego-Varillas, R.; Scotognella, F.; Kriegel, I.; Yan, A.; Zettl, A.; Schuck, P. J.; Knorr, A.; Cerullo, G.; Conte, S. D., The Ultrafast Onset of Exciton Formation in 2D Semiconductors. *Nat. Commun.* **2020**, *11*, 5277.
76. Wang, Z.; Altmann, P.; Gadermaier, C.; Yang, Y.; Li, W.; Ghirardini, L.; Trovatiello, C.; Finazzi, M.; Duo, L.; Celebrano, M.; Long, R.; Akinwande, D.; Prezhdoo, O. V.; Cerullo, G.; Dal Conte, S., Phonon-Mediated Interlayer Charge Separation and Recombination in a MoSe₂/WSe₂ Heterostructure. *Nano Lett.* **2021**, *21*, 2165-2173.
77. Reichardt, S.; Wirtz, L., Nonadiabatic Exciton-Phonon Coupling in Raman Spectroscopy of Layered Materials. *Sci. Adv.* **2020**, *6*, eabb5915.
78. Carvalho, B. R.; Wang, Y.; Mignuzzi, S.; Roy, D.; Terrones, M.; Fantini, C.; Crespi, V. H.; Malard, L. M.; Pimenta, M. A., Intervalley Scattering by Acoustic Phonons in Two-Dimensional MoS₂ Revealed by Double-Resonance Raman Spectroscopy. *Nat. Commun.* **2017**, *8*, 14670.
79. Kioseoglou, G.; Hanbicki, A. T.; Currie, M.; Friedman, A. L.; Gunlycke, D.; Jonker, B. T., Valley Polarization and Intervalley Scattering in Monolayer MoS₂. *Appl. Phys. Lett.* **2012**, *101*, 221907.
80. Sie, E. J.; Lui, C. H.; Lee, Y. H.; Kong, J.; Gedik, N., Observation of Intervalley Biexcitonic Optical Stark Effect in Monolayer WS₂. *Nano Lett.* **2016**, *16*, 7421-7426.

81. Gao, F.; Gong, Y.; Titze, M.; Almeida, R.; Ajayan, P. M.; Li, H., Valley Trion Dynamics in Monolayer MoSe₂. *Phys. Rev. B* **2016**, *94*, 245413.
82. Hao, K.; Xu, L.; Nagler, P.; Singh, A.; Tran, K.; Dass, C. K.; Schuller, C.; Korn, T.; Li, X.; Moody, G., Coherent and Incoherent Coupling Dynamics between Neutral and Charged Excitons in Monolayer MoSe₂. *Nano Lett.* **2016**, *16*, 5109-5113.
83. Singh, A.; Moody, G.; Tran, K.; Scott, M. E.; Overbeck, V.; Berghäuser, G.; Schaibley, J.; Seifert, E. J.; Pleskot, D.; Gabor, N. M.; Yan, J.; Mandrus, D. G.; Richter, M.; Malic, E.; Xu, X.; Li, X., Trion Formation Dynamics in Monolayer Transition Metal Dichalcogenides. *Phys. Rev. B* **2016**, *93*, 041401.
84. Tempelaar, R.; Berkelbach, T. C., Many-Body Simulation of Two-Dimensional Electronic Spectroscopy of Excitons and Trions in Monolayer Transition Metal Dichalcogenides. *Nat. Commun.* **2019**, *10*, 3419.
85. Singh, A.; Tran, K.; Kolarczik, M.; Seifert, J.; Wang, Y.; Hao, K.; Pleskot, D.; Gabor, N. M.; Helmrich, S.; Owschimikow, N.; Woggon, U.; Li, X., Long-Lived Valley Polarization of Intravalley Trions in Monolayer WSe₂. *Phys. Rev. Lett.* **2016**, *117*, 257402.
86. Titze, M.; Li, B.; Zhang, X.; Ajayan, P. M.; Li, H., Intrinsic Coherence Time of Trions in Monolayer MoSe₂ Measured via Two-Dimensional Coherent Spectroscopy. *Phys. Rev. Mater.* **2018**, *2*, 054001.
87. Feng, S.; Cong, C.; Konabe, S.; Zhang, J.; Shang, J.; Chen, Y.; Zou, C.; Cao, B.; Wu, L.; Peimyoo, N.; Zhang, B.; Yu, T., Engineering Valley Polarization of Monolayer WS₂: A Physical Doping Approach. *Small* **2019**, *15*, e1805503.
88. Miyauchi, Y.; Konabe, S.; Wang, F.; Zhang, W.; Hwang, A.; Hasegawa, Y.; Zhou, L.; Mouri, S.; Toh, M.; Eda, G.; Matsuda, K., Evidence for Line Width and Carrier Screening Effects on Excitonic Valley Relaxation in 2D Semiconductors. *Nat. Commun.* **2018**, *9*, 2598.
89. Shinokita, K.; Wang, X.; Miyauchi, Y.; Watanabe, K.; Taniguchi, T.; Matsuda, K., Continuous Control and Enhancement of Excitonic Valley Polarization in Monolayer WSe₂ by Electrostatic Doping. *Adv. Funct. Mater.* **2019**, *29*, 1900260.
90. Lin, W. H.; Tseng, W. S.; Went, C. M.; Teague, M. L.; Rossman, G. R.; Atwater, H. A.; Yeh, N. C., Nearly 90% Circularly Polarized Emission in Monolayer WS₂ Single Crystals by Chemical Vapor Deposition. *ACS Nano* **2020**, *14*, 1350-1359.
91. Rosenberger, M. R.; Chuang, H. J.; McCreary, K. M.; Li, C. H.; Jonker, B. T., Electrical Characterization of Discrete Defects and Impact of Defect Density on Photoluminescence in Monolayer WS₂. *ACS Nano* **2018**, *12*, 1793-1800.
92. McCreary, K. M.; Currie, M.; Hanbicki, A. T.; Chuang, H.-J.; Jonker, B. T., Understanding Variations in Circularly Polarized Photoluminescence in Monolayer Transition Metal Dichalcogenides. *ACS Nano* **2017**, *11*, 7988-7994.

93. Kolesnichenko, P. V.; Zhang, Q.; Yun, T.; Zheng, C.; Fuhrer, M. S.; Davis, J. A., Disentangling the Effects of Doping, Strain and Disorder in Monolayer WS₂ by Optical Spectroscopy. *2D Mater.* **2020**, *7*, 025008.
94. Wang, H.; Zhang, C.; Rana, F., Ultrafast Dynamics of Defect-Assisted Electron-Hole Recombination in Monolayer MoS₂. *Nano Lett.* **2015**, *15*, 339-345.
95. Kang, K.; Lee, K.-H.; Han, Y.; Gao, H.; Xie, S.; Muller, D. A.; Park, J., Layer-by-Layer Assembly of Two-Dimensional Materials into Wafer-Scale Heterostructures. *Nature* **2017**, *550*, 229-233.
96. Kaasbjerg, K.; Martiny, J. H. J.; Low, T.; Jauho, A.-P., Symmetry-Forbidden Intervalley Scattering by Atomic Defects in Monolayer Transition-Metal Dichalcogenides. *Phys. Rev. B* **2017**, *96*, 241411.
97. Zheng, H.; Caram, J. R.; Dahlberg, P. D.; Rolczynski, B. S.; Viswanathan, S.; Dolzhenkov, D. S.; Khadivi, A.; Talapin, D. V.; Engel, G. S., Dispersion-Free Continuum Two-Dimensional Electronic Spectrometer. *Appl. Opt.* **2014**, *53*, 1909-1917.
98. Dahlberg, P. D.; Fidler, A. F.; Caram, J. R.; Long, P. D.; Engel, G. S., Energy Transfer Observed in Live Cells Using Two-Dimensional Electronic Spectroscopy. *J. Phys. Chem. Lett.* **2013**, *4*, 3636-3640.
99. Jonas, D. M., Two-Dimensional Femtosecond Spectroscopy. *Annu. Rev. Phys. Chem.* **2003**, *54*, 425-463.
100. Lloyd, L. T.; Wood, R. E.; Allodi, M. A.; Sohoni, S.; Higgins, J. S.; Otto, J. P.; Engel, G. S., Leveraging Scatter in Two-Dimensional Spectroscopy: Passive Phase Drift Correction Enables a Global Phasing Protocol. *Opt. Express* **2020**, *28*, 32869-32881.
101. Momma, K.; Izumi, F., Vesta 3 for Three-Dimensional Visualization of Crystal, Volumetric and Morphology Data. *J. Appl. Crystallogr.* **2011**, *44*, 1272-1276.